SIMULATION OF FLAME TEMPERATURE RECONSTRUCTION THROUGH MULTI-PLENOPTIC CAMERA TECHNIQUES

Qi Qi[1], M. M. Hossain[2], C. Xu[1*], B. Zhang[1], J. Sun[3]

[1]Key Laboratory of Energy Thermal Conversion and Control of Ministry of Education, School of Energy and Environment, Southeast University, 210018, Nanjing, China
[2]School of Engineering and Digital Arts, University of Kent, Canterbury, Kent, CT2 7NT, UK
[3]Sunny Central Research Institute, No.1190, Bin'an Road, Binjiang District, Hangzhou, China

[*]Email: chuanlongxu@seu.edu.cn

ABSTRACT

Due to the variety of burner structure and fuel mixing, the flame temperature distribution is not only manifold but also complex. Therefore, it is necessary to develop an advanced temperature measurement technique, which can provide not only the adequate flame radiative information but also reconstruct the complex temperature accurately. This paper presents a comprehensive simulation of flame temperature reconstruction through multi-plenoptic camera techniques. A novel multi-plenoptic camera imaging technique is proposed which is able to provide adequate flame radiative information only from two different directions and to reconstruct the three dimensional (3D) temperature of a flame. An inverse algorithm i.e., Non-negative Least Squares is used to reconstruct the flame temperature. To verify the reconstruction algorithm, two different temperature distributions such as unimodal axisymmetric and bimodal asymmetric are used. Numerical simulations are carried out to evaluate the performance of the technique. It has been observed that the reconstruction accuracy decreases with the increasing of signal-to-noise ratios. However, compared with the single plenoptic and conventional multi-camera techniques, the proposed method has the advantages of lower relative error and better reconstruction quality and stability even with the higher SNRs for both temperature distributions. Therefore, the proposed multi-plenoptic camera imaging technique is capable of reconstructing the complex 3-D temperature fields more accurately.

Keywords flame reconstruction, non-negative least squares, plenoptic camera, temperature

Industrial Application General

1 INTRODUCTION

Combustion is widely applied in industrial processes such as power plants, aerospace engineering, solid propellant rockets, and ferrous metallurgy. The accurate measurement of the flame temperature would be significant to adjust the combustion mode, optimize the combustion process and control the pollutant emissions (NOx and CO). Due to the variety of burner structures and fuel mixing, the characteristics of the flame become complex. Therefore, it is desirable to develop an advanced measurement technique that can provide not only the adequate flame radiative information but also reconstruct the complex such as multi-peak flame temperature accurately. Over the past years, various measurement techniques were developed to obtain the flame temperature (Zhou，2005). They are mainly categorised into intrusive and non-intrusive techniques. For instance, thermocouple is a typical intrusive, simple and intuitive temperature measurement technique and it measures the flame temperature point by point. In addition, it affects the original structure of the flame thus the temperature distribution and combustion process (Yilmaz N, 2008, Hindasageri V, 2013). Therefore, this technique is restricted in many industrial processes. In contrast, the non-intrusive measurement techniques do not directly contact with the flame and do not interfere with the temperature distribution in the combustion process.

Various non-intrusive measurement techniques were reported based on acoustic computed tomography (CT), laser-based and radiative imaging (Zheng L, 2011; Denisov A, 2014; Tolles W M, 1977; Cheng Q, 2014). For example, Zhang et al. (2015) used an acoustic CT to monitor the cross-sectional temperature of a boiler furnace and the temperature was reconstructed through an iterative algebraic reconstruction technique (ART). Yang et al. (2015) utilized a multiplexed tunable diode laser

absorption spectroscopy (TDLAS) technique to obtain spatially resolved temperature information from a low-pressure premixed flame reactor. Although the acoustic CT techniques have been attracted extensive attention to the scientists, difficult to acquire 3-D temperature profile due to poor resistance to high temperature. Besides, due to the complexity of optical path and higher cost of the system, the laser-based techniques are generally not suitable for abominably industrial environments. Among those techniques, the radiative imaging-based techniques have been recognized as effective and accurate for the flame temperature measurement. In addition, they are relatively simple in system setup, cost-effective and easy to manipulate for industrial environments. Based on sensing devices and computational techniques, they are divided into single-camera and multi-camera imaging techniques. For instance, Brisely et al. (2005) proposed a single-camera technique to reconstruct the cross-sectional temperature of a gas flame. Y. Lu (1998) also utilized a single-camera technique to measure the 3-D temperature of a flame. The single-camera techniques are simple but unable to reconstruct complex and turbulent flames temperature. Only suitable for stable or rotational symmetrical flames. The multi-camera techniques utilize multiple sensing devices (i.e., CCD/CMOS or optical imaging fibres) to obtain multiple perspective projections from different directions of a flame and to reconstruct the flame temperature. For example, Hossain et al. (2012, 2013) proposed a multi-camera technique based on optical fibre sensing integrating CT and two-color pyrometry to reconstruct grey-level intensity and temperature of the flame. Zhou et al. (2005) developed a system with eight image detectors to capture monochromatic radiation intensity of a pulverized-coal-fired flame. Cheng et al. (2014) utilized four CCD detectors to reconstruct the 3-D temperature distribution of a gas-fired pilot tubular furnace flame. Floyd et al. (2011) used five cameras and number of mirrors located uniformly around the burner to obtain 48 projections of the flame. Although the multi-camera techniques are able to acquire more radiative information and to reconstruct complex flame temperature, they are complex in setup, high cost due to the increase of multiple sensing devices. Also, a high degree of coupling and synchronization are required for the multi-camera techniques.

In recent years, the single plenoptic camera (light field) technique has been attracting significant attention (Georgiev T G, 2010) in the area of combustion monitoring due to its capability of acquiring directions and positions information of the flame simultaneously in a single exposure. For instance, Sun et al. (2016) applied a single light field camera to record 3-D radiative information of ethylene diffusion flame and the least square QR-factorization algorithm (LSQR) is used to reconstruct the flame temperature through simulations and experiments. Zhao et al. (2017) proposed an optical sectioning tomography along with a single light field imaging technique to reconstruct the 3-D flame temperature. Huang et al. (2018) also used a single plenoptic camera with Landweber method to reconstruct the 3-D temperature distribution. Although the single plenoptic camera is able to record directions and positions information of the flame simultaneously, however, the directional difference of the radiative information recorded by the single plenoptic camera is limited and thus rendering similar radiative information of the flame for the temperature reconstruction. The ill-conditioning and mathematical ambiguity will also worsen to solve the radiative information accurately and result in the lower accuracy and resolution, especially for complex and turbulent flames. More radiative information with a larger directional difference and higher resolution are required to achieve accurate flame temperature measurement. The motivations of this study are to investigate numerically flame radiative information for temperature reconstruction through multi-plenoptic camera techniques and to compare reconstruction accuracy with the single plenoptic and conventional multi-camera techniques.

This study presents a novel method to reconstruct the 3-D temperature of a flame based on multi-plenoptic cameras (i.e., two) and the numerical simulations. A plenoptic imaging model is developed to acquire the flame radiative information and a Non-negative Least Squares (NNLS) algorithm is used to reconstruct the temperature. Feasibility and practicality of the techniques are evaluated through the simulations. The evaluation of the proposed technique is also carried out under unimodal symmetrical and bimodal asymmetrical flames temperature distribution with different signal-to-noise ratios (SNRs). The results obtained from the proposed technique are presented. The results also compared with the single plenoptic camera and the conventional multi-camera techniques and discussed.

2 PROPOSED TECHNIQUE

2.1 System description

Figure 1 shows a schematic diagram of the proposed multi-plenoptic camera system. The system consists of two identical plenoptic cameras and a computer with application software. Two plenoptic

cameras are placed at two different angles (0° and 45°) around the flame to obtain flame radiativ e information. In the plenoptic camera, a microlens array is installed between the photosensor and the main lens. The photosensor of the plenoptic camera deviates from the focal plane of the microlens array. The plenoptic camera thus reduces the dimension of the directional sampling and improves the dimension of the spatial sampling. The directional radiative intensity of the whole field of view (FOV) is obtained by ray tracing technique. In order to achieve this, a pinhole camera model is used to trace the rays. The radiative rays traced from the sensor pixels to the flame. The parameters of the plenoptic camera used in this study are shown in Table 1.

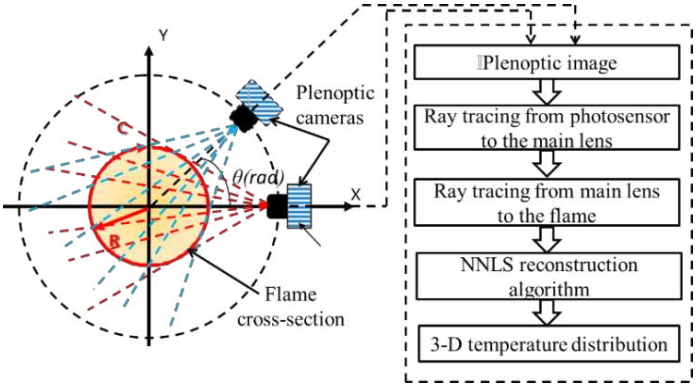

Figure 1. Schematic of the multi-plenoptic camera system

Table 1. Parameters of plenoptic camera

Symbol	Description	Value
L_{om} (mm)	the distance between flame centerline to the main lens	505
L_{mm} (mm)	the distance between main lens and microlens array	53.1
L_{mp} (μm)	the distance between microlens array and photosensor	480
f (mm)	the focal length of the main	50
f_m (μm)	the focal length of the microlens	600
N_m	number of microlenses	60×60
N_p	number of pixels covered by each microlens array	12
d_p (μm)	length of the pixels	8
d_m (μm)	the diameter of each microlens	95

To compare the results obtained by the proposed system and the conventional multi-camera system, two conventional CCD cameras are also placed in the similar locations to obtain the flame radiative information. The focal length of the main lens of the conventional camera is 50 mm, the distance between flame centerline to the main lens is 505 mm, the distance between the main lens and the photosensor is 55.5 mm.

3 MEASUREMENT PRINCIPLE

3.1 Plenoptic Imaging Model

As shown in Fig. 2, a subject of interest at the desired depth is imaged in both the conventional and the light field cameras. In a conventional camera, rays from a single point on the subject are brought to a single convergence point on the photosensor. However, rays from a single point on the subject are brought to a single convergence point on the virtual image plane of the main lens in light field camera. Then the microlens separates these rays based on direction, creating a focused image on the array of pixels underneath the microlens. It is important to establish a plenoptic imaging model to acquire directional radiative information from the whole FOV of the plenoptic image. To achieve that a plenoptic imaging model is proposed in this study. The plenoptic imaging model divided into; 1) imaging by the main lens and 2) imaging by the microlens array. To obtain the directional radiative information of the whole FOV, the ray must be traced from the pixel to the object. It can be determined by the main lens plane and microlens array in the plenoptic camera. As shown in Figure 2, the pixel point 2 and virtual image point 1 is conjugated for the corresponding microlens and their center is point

3. Also, point 1 and virtual point 5 is conjugated for the main lens and their center is point 0. Therefore, the coordinate (x_1, y_1, z_1) of point 1 can be derived from the following equations;

$$\frac{1}{L_{mp}}+\frac{1}{L_{mv}}=\frac{1}{f_m} \tag{1}$$

$$\frac{z_3-z_2}{z_3-z_1}=\frac{y_3-y_2}{y_3-y_1}=\frac{L_{mp}}{L_{mv}} \tag{2}$$

where (x_2, y_2, z_2) is the coordinate of point 2, (x_3, y_3, z_3) is the coordinate of point 3. L_{mv} is the distance between the virtual image plane and the microlens array. Similar way, the coordinate (x_5, y_5, z_5) of point 5 can be calculated by;

$$\frac{1}{L_{om}}+\frac{1}{L_{mv}+L_{mm}}=\frac{1}{f} \tag{3}$$

$$\frac{z_0-z_1}{z_5-z_0}=\frac{y_0-y_1}{y_5-y_0}=\frac{L_{mv}+L_{mm}}{L_{om}} \tag{4}$$

where (x_0, y_0, z_0) is the coordinate of point 0. The direction of the flame radiation with the known coordinates of the point 4 and 5 can be calculated by,

$$\theta=\arccos\left[\frac{(z_4-z_5)}{\sqrt{L_{om}{}^2+(y_4-y_5)^2+(z_4-z_5)^2}}\right] \tag{5}$$

$$\psi=\begin{cases}\arctan\left(\dfrac{y_4-y_5}{x_4-x_5}\right), y_4\geq y_5\\ \arctan\left(\dfrac{y_4-y_5}{x_4-x_5}\right)+2\pi, y_4<y_5\end{cases} \tag{6}$$

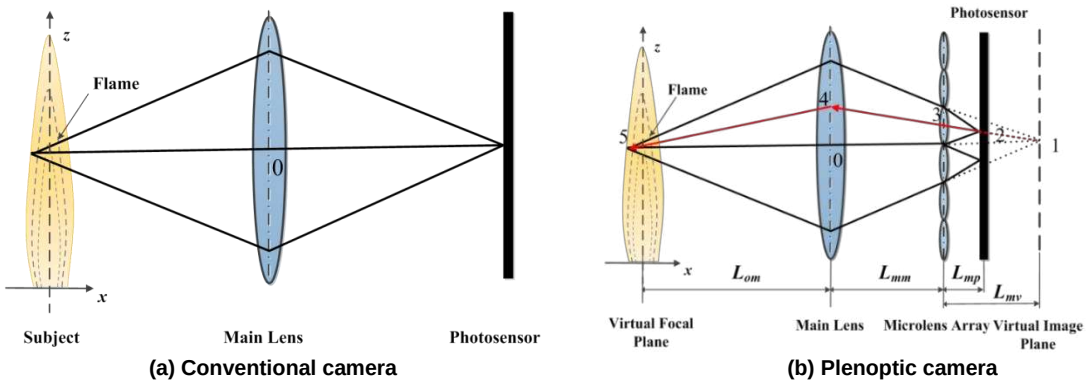

(a) Conventional camera **(b) Plenoptic camera**

Figure 2. Schematic of flame radiation sampling with a conventional camera and plenoptic camera

3.2 A mathematical model for flame temperature

The intensity detected from a pixel is regarded as the intensity of the ray, which can be calculated using Radiative Transfer Equation (RTE). Based on the Mie theory, the scattering of soot particles is far less than the absorption in flames (Felske J D, 1973), therefore, in this study, the scattering is ignored and only the absorption is taken into consideration. Hence, taking the intensity of the ray along the path L as an example, the steady-state RTE can be simplified as follows;

$$\frac{\mathrm{d}\, I_{\lambda}^{L}}{\mathrm{d}\,\tau_{L}} = -I_{\lambda}^{L} + I_{b\lambda} \tag{7}$$

where I_{λ}^{L} is the final radiation intensity of the flame for path L, $I_{b\lambda}$ and τ_L are the blackbody radiation intensity and the optical thickness of the voxel. τ_L is equal to the integral of the absorption coefficient within the length. Equation 7 can be written as a linear equation as follows:

$$I_{\lambda}^{\ m} = \sum_{i=1}^{n} A_{m}^{vi} I_{b\lambda}^{vi} \tag{8}$$

$$\begin{cases} A_{m}^{vi} = \exp(-\sum_{j=i+1}^{n} \tau_{vj}) - \exp(-\sum_{j=i}^{n} \tau_{vj}) & i < n \\ A_{m}^{vi} = 1 - \exp(-\sum_{j=i}^{n} \tau_{vj}) & i = n \end{cases} \tag{9}$$

$$\mathbf{I}_{\lambda} = \mathbf{A} \cdot \mathbf{I}_{b\lambda} \tag{10}$$

where m is the number of final radiation ray L, $\mathbf{I}_{\lambda}$ is the radiation intensity detected by the photosensor, n is the total number of the voxel that the radiation ray passes through, **A** is the coefficient matrix.

3.3 Inverse algorithm

In the inverse problem, the radiative intensities received by the photosensor $\mathbf{I}_{\lambda}$ regarded as input, the temperature field can be obtained based on the blackbody radiative intensity $\mathbf{I}_{b\lambda}$ and Planck's law. The dependence of blackbody radiative intensity $\mathbf{I}_{b\lambda}$ and the temperature T is expressed by Eq. (11). Due to the pixels covered by the fame image is high, so the RTEs composed by Eq. (10) is enormous. Meanwhile, the number of the voxel that each ray crosses through is far less than the total number of the voxel, result in a sparse large and ill-conditioned matrix **A** with a large number of zeros. This paper utilizes the Non-Negative Least Squares (NNLS) algorithm to solve these problems. In this method, when the selected component is negative, sets it to zero and continue iterates until converge. It can guarantee the non-negativity of the result and it possesses good stability. The detailed procedures of the NNLS algorithm can be found in Ref. (LAWSON C L, 1995).

$$I_{b\lambda}(r) = c_1 \lambda^{-5} \Big/ \pi \left[e^{\frac{c_2}{\lambda T(r)}} - 1 \right] \tag{11}$$

where c_1 is the first radiation constant, 3.7418×10^{-16} W·m^2, c_2 is the second radiation constant, 1.4388×10^{-2} m·K, λ is the wavelength of the flame radiation. T(r) is the temperature at the location r, K.

4 NUMERICAL SIMULATION

To evaluate the performance of the proposed system, numerical simulations are carried out to reconstruct the flame temperature. Two different flame temperature distributions are used and described in Sections 4.1 and 4.2. The simulated flame is considered as a cylindrical and the temperature range is set to 1000 – 2000 K. The radius (R) and axial length (Z) of the simulated flame are 0.008 m and 0.03 m, respectively. The cylindrical flame is divided into 432 grids, that is $N_{\phi} \times N_r \times N_z = 12 \times 6 \times 6$. The absorption coefficient of 10 m^{-1} used in this study is based on the Ref. (Santoro R J, 1987). The simulations are also carried out for the single plenoptic camera (placed at 45°) and the conventional multi-camera systems. Their results are compared with the proposed system.

4.1 Unimodal axisymmetric temperature distribution

To verify the proposed technique, the unimodal axisymmetric temperature field of the simulated flame is assumed to be a function of r and z and can be expressed by Eq. (12) (Huang X, 2018).

$$T(r,z)=1200\exp\left\{-\left[3\left(\frac{r^2}{R^2}+\frac{z^2}{Z^2}\right)-0.9\right]^2\right\}+900\ [K] \tag{12}$$

where r and z are the radial and axial coordinates of the coordinate system, respectively. The temperature distribution obtained from the (12) is shown in Figure 3 as cross-sectional and longitudinal distributions.

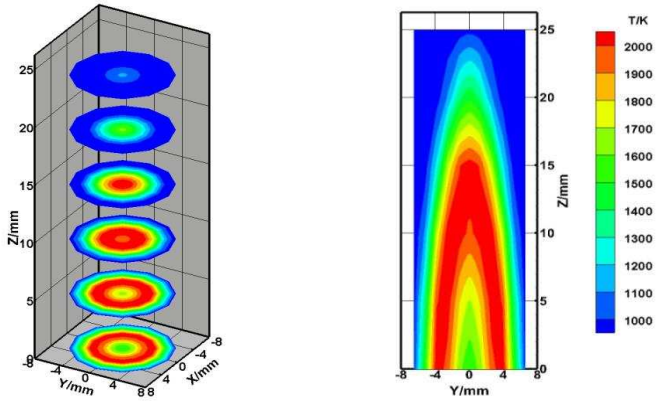

(a) Cross-sections (b) Longitude-section, X = 0 mm

Figure 3. The temperature distribution of a unimodal axisymmetric flame

4. 2 Bimodal asymmetric temperature distribution

The proposed technique is also evaluated under complex flame temperature distribution. In practical, the flame is complex and asymmetric. Therefore, it is required to examine the practicality and performance of the proposed technique under asymmetric and complex temperature distribution. To achieve that a bimodal asymmetric temperature distribution which has two-peak flame temperature is considered. It can be defined as follows (Niu C Y, 2016);

$$T(x,y,z)=\frac{2200}{3}\left\{\begin{array}{l}\exp\left\{-40\left[(750x+7.5)/9-1.1\right]^2-25\left[(750y+8.5)/9-0.8\right]^2\right\}\\+0.8\exp\left\{-25\left[(750x+7.5)/9-0.8\right]^2-35\left[(750y+8.5)/9-1.2\right]^2\right\}\end{array}\right\}$$
$$+880(1-100z/3)+753\ [K] \tag{13}$$

where x, y and z are the coordinates of the coordinate system, respectively. The bimodal asymmetric temperature distribution derived from the (13) is shown in Figure 4.

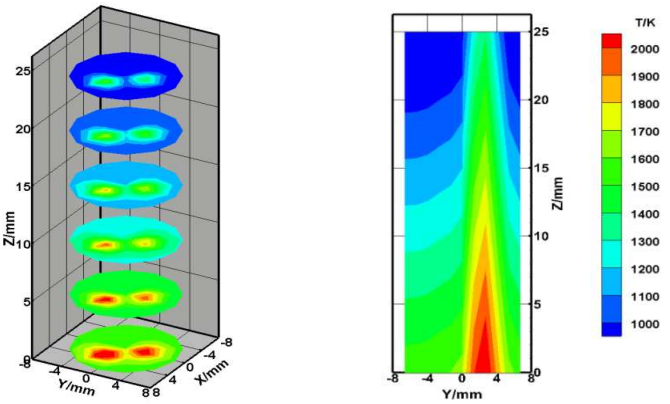

(a) Cross-sections (b) Longitude-section, X = 0 mm

Figure 4. The temperature distribution of a bimodal asymmetric flame

4.3 Effects of Noise and Error Calculation

In order to investigate the performance of the technique under different noises, the Gaussian noises i.e., signal-to-noise ratios (SNRs) are added to the flame radiative intensity. In this study, the SNR = 1dB, 10dB and 20 dB are considered. The SNR is defined as follows;

$$\mathrm{SNR} = 10\log_{10}\left[\sum_{i=1}^{k}\left(I_{\lambda}^{i}\right)^{2} \Big/ \sum_{i=1}^{k}\left(N_{i}\right)^{2}\right] \tag{14}$$

where I_{λ}^{i} is the spectral radiative intensity of the i^{th} pixel of the photosensor, N_i is the noise value of the i^{th} pixel of the photosensor, k is the number of pixels of the photosensor. To evaluate the performance, the relative error of the reconstructed temperature ΔT is defined as follows;

$$\Delta T = \frac{\left|T_{rst} - T_{ori}\right|}{T_{ori}} \tag{15}$$

where T_{rst} is the reconstructed temperature, T_{ori} is the original temperature.

5 RESULTS AND DISCUSSION

Figures 5 and 6 show the simulated flame images obtained for the plenoptic and the conventional multi-camera systems. As shown in Figure 5, the flame radiative intensity is similar at angles 0° and 45° for the unimodal axisymmetric condition. It can be seen that the radiative intensity distribution is not continuous due to the microlens array in the plenoptic camera. On the contrary, the radiative distribution is continuous for the conventional camera. For the bimodal asymmetric condition, the distribution of the flame radiative intensity is non-uniform at angles 0º and 45º as shown in Figure 6. Where the simulated flame images manifest the complex temperature distribution at different angles.

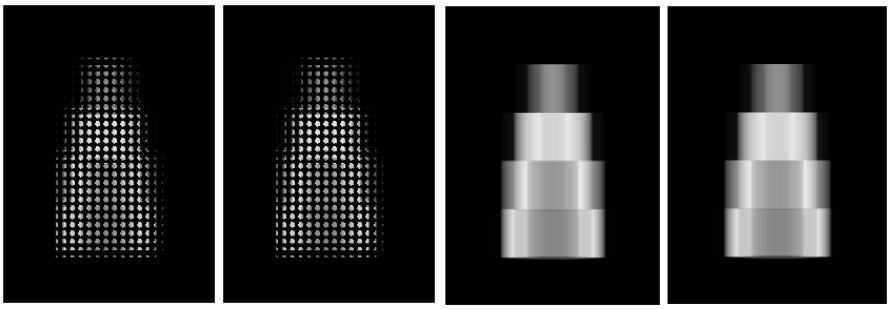

Figure 5. Simulated flame images at different angles under unimodal axisymmetric

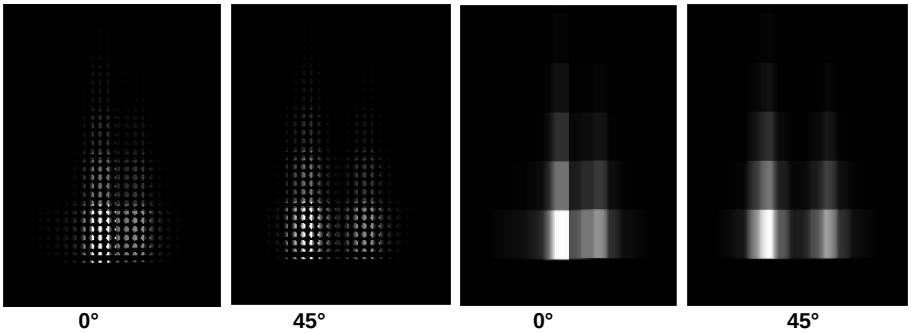

Figure 6. Simulated flame images at different angles under bimodal asymmetric

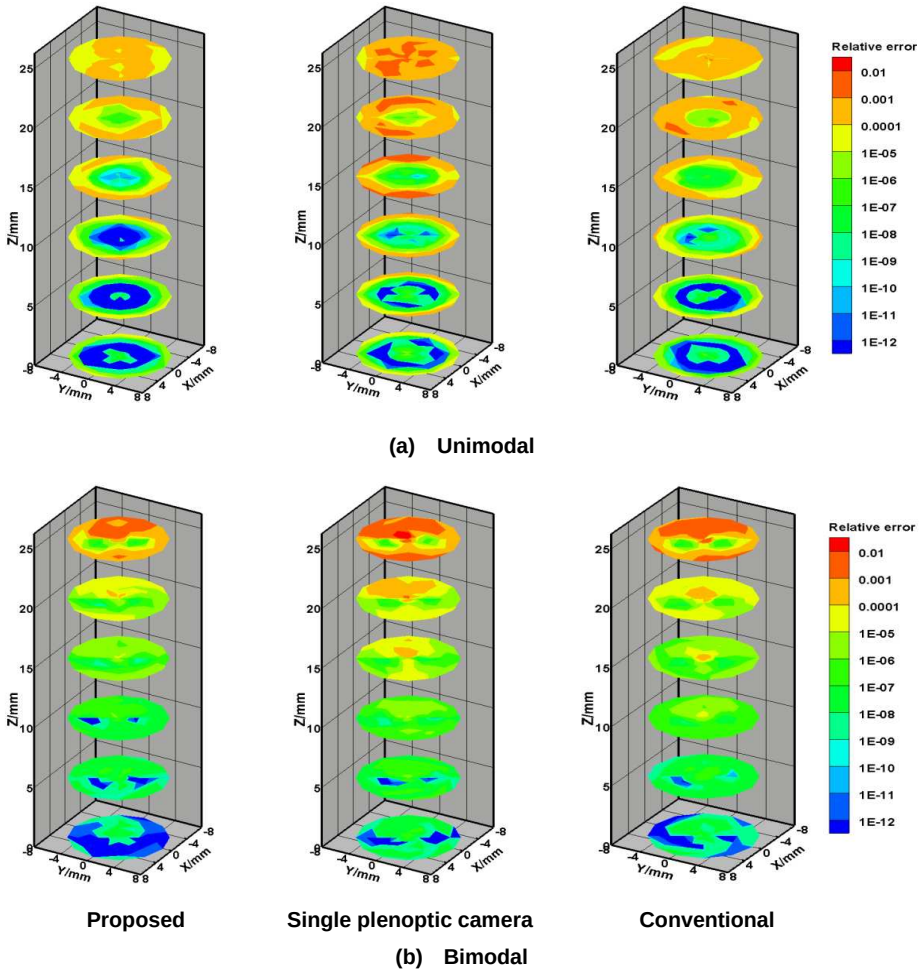

Figure 7. The reconstructed relative error distributions of simulated flame temperature at SNR = 1 dB.

Figure 7 shows the distribution of reconstructed relative error of the unimodal axisymmetric and bimodal asymmetric flame temperature at SNR = 1 dB. It can be seen that the better reconstruction quality is achieved for the proposed technique compared to the single and conventional multi-camera techniques, especially in the high-temperature regions. For unimodal axisymmetric, the maximum reconstruction error is 7.6×10^{-4} for the proposed technique, however, 6.7×10^{-3} and 2×10^{-2} for the single plenoptic camera and the conventional multi-camera techniques, respectively. The mean relative errors of the reconstructed unimodal axisymmetric and bimodal asymmetric flame temperature are shown in Figure 8. It has been observed that the reconstruction error decreases with the increasing of SNRs. The results obtained from this study demonstrate that the bimodal asymmetric flame temperature can be measured accurately by the multi-plenoptic camera technique even with the higher noises.

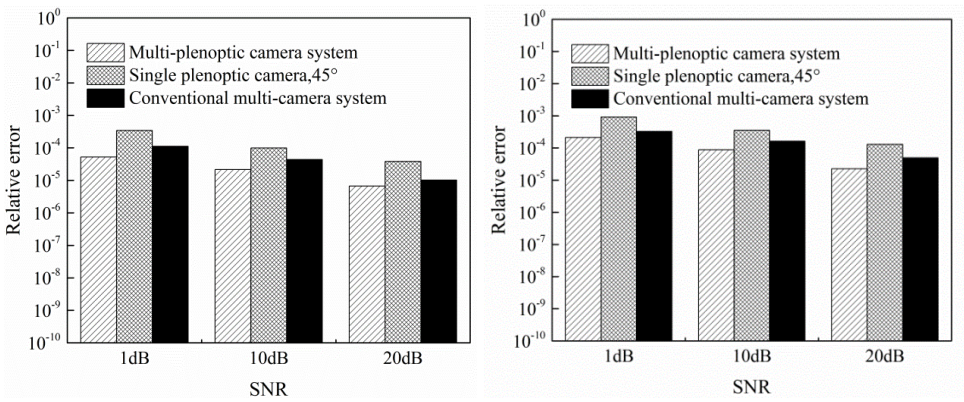

(a) Unimodal **(b) Bimodal**

Figure 8. The mean relative error of temperature with different noises

6 CONCLUSIONS

In this paper, a multi-plenoptic camera technique is proposed to reconstruct the flame temperature. Numerical simulations are carried out for the proposed technique. A plenoptic imaging model is developed to obtain the directional radiative intensity of the flame. The non-negative least square algorithm is used to reconstruct the simulated flame temperature. The results showed that the flame temperature can be reconstructed accurately by the proposed technique and the reconstruction accuracy remains higher even with the SNR = 1 dB. The mean relative error is calculated to evaluate the system. The mean relative error is smaller for the unimodal and bimodal temperature distributions compared to single plenoptic and conventional multi-camera techniques. Also, the better reconstruction quality is achieved by the proposed technique. Thus, the more accurate flame temperature can be obtained and the proposed technique has the potential to be applied to measure the complex, manifold and irregular flames.

Acknowledgements

This work is supported by the National Natural Science Foundation of China [grant numbers 51676044 51506030 51327803]; Natural Science Foundation of Jiangsu Province for Distinguished Young Scholars [grant number, BK20150023].

REFERENCES

BRISLEY P M, LU G, YAN Y, et al., (2004) Three-dimensional temperature measurement of combustion flames using a single monochromatic CCD camera, IEEE T INSTRUM MEAS., 2005 54 p1417-1421; DOI: 10.1109/TIM.2005.851074.

CHENG Q, ZHANG X, WANG Z, et al., (2014) Simultaneous Measurement of Three-Dimensional Temperature Distributions and Radiative Properties Based on Radiation Image Processing Technology in a Gas-Fired Pilot Tubular Furnace, Heat Transfer Eng., 2014 35 p770-779; DOI: 10.1080/08832323.2013.838096.

DENISOV A, COLMEGNA G, JANSOHN P, (2014) Temperature measurements in sooting counterflow diffusion flames using laser-induced fluorescence of flame-produced nitric oxide, Appl. Phys. B, 2014 116 p339-346; DOI: 10.1007/s00340-013-5697-6.

FELSKE J D, TIEN C L, (1973) Calculation of the Emissivity of Luminous Flames, Combust. Sci. Technol., 1973 7 p25-31; DOI: 10.1080/00102207308952339.

FLOYD J, KEMPF A M, (2011) Computed Tomography of Chemiluminescence (CTC): High resolution and instantaneous 3-D measurements of a Matrix burner, Proc. Combust. Inst., 2011 33 p751-758; DOI: 10.1016/j.proci.2010.06.015.

GEORGIEV T G, LUMSDAINE A, (2010) Focused plenoptic camera and rendering, J. Electron. Imaging, 2010 19 021106; DOI: 10.1117/1.3442712.

HINDASAGERI V, VEDULA R P, PRABHU S V, (2013) Thermocouple error correction for measuring the flame temperature with determination of emissivity and heat transfer coefficient, Rev. Sci. Instrum., 2013 84 024902; DOI: 10.1063/1.4790471.

HOSSAIN M M, LU G, SUN D, et al., (2013) Three-dimensional reconstruction of flame temperature and emissivity distribution using optical tomographic and two-colour pyrometric techniques, Meas. Sci. Technol., 2013 24 074010; DOI: 10.1088/0957-0233/24/7/074010.

HOSSAIN M M, LU G, YAN Y, (2012) Optical Fiber Imaging Based Tomographic Reconstruction of Burner Flames, IEEE Trans. Instrum. Meas., 2012 61 p1417-1425; DOI: 10.1109/TIM.2012.2186477.

HUANG X, QI H, ZHANG X L, et al., (2018) Application of Landweber Method for Three-Dimensional Temperature Field Reconstruction Based on the Light-Field Imaging Technique, J. Heat Transfer, 2018 140 082701; DOI: 10.1115/1.4039305.

LAWSON C L, HANSON R J, (1995) Solving Least Square Problems, Prentice Hall, ISBN: 0-89871-365.

LU Y, WANG S, (1998) 3-Dimensional Irradiance imaging with a single camera system, Southeast. Univ. English. Ed, 1998 14 p40–44.

LUMSDAINE A, GEORGIEV T G, CHUNEV G, (2012), Spatial analysis of discrete plenoptic sampling. IS&T/SPIE Electronic Imaging, California, United States, 8299 829909.

NIU C Y, QI H, HUANG X, et al., (2016) Efficient and robust method for simultaneous reconstruction of the temperature distribution and radiative properties in absorbing, emitting, and scattering media, J. Quant. Spectrosc. Radiat. Transfer, 2016 184 p44-57; DOI: 10.1016/j.jqsrt.2016.06.032.

SANTORO R J, et al., (1987) The Transport and Growth of Soot Particles in Laminar Diffusion Flames, COMBUST. SCI. TECHNOL, 1987 53 p89-115; DOI: 10.1080/00102208708947022.

SUN J, XU C, ZHANG B, et al., (2016) Three-dimensional temperature field measurement of flame using a single light field camera, Opt. Express, 2016 24 p1118-1132; DOI: 10.1364/oe.24.001118.

TOLLES W M, NIBLER J W, MCDONALD J R, et al., (1977) A Review of the Theory and Application of Coherent Anti-Stokes Raman Spectroscopy (CARS), Appl. Spectrosc., 1977 31 p253-271; DOI: 10.1366/000370277774463625.

YANG H N, YANG B, CAI X S, et al., (2015) Three-Dimensional (3-D) Temperature Measurement in a Low Pressure Flame Reactor Using Multiplexed Tunable Diode Laser Absorption Spectroscopy (TDLAS), Lasers in Eng., 2015 31 p285-297

YILMAZ N, GILL W, DONALDSON A B, et al., (2008) Problems Encountered in Fluctuating Flame Temperature Measurements by Thermocouple, Sensors, 2008 8 p7882-7893; DOI: 10.3390/s8127882.

ZHANG S, SHEN G, AN L, et al., (2015) Online monitoring of the two-dimensional temperature field in a boiler furnace based on acoustic computed tomography, Appl. Therm. Eng., 2015 75 p958-966; DOI: 10.1016/j.applthermaleng.2014 10 085.

ZHAO W, ZHANG B, XU C, et al., (2017) Optical Sectioning Tomographic Reconstruction of Three-dimensional Flame Temperature Distribution Using Single Light Field Camera, IEEE SENS J., 2017 18 p528 – 539;DOI: 10.1109/JSEN.2017.2772899.

ZHENG L, (2011) Oxy-Fuel Combustion for Power Generation and Carbon Dioxide (CO2) Capture, Woodhead Publishing, ISBN: 978-1-84569-671-9.

ZHOU H C, LOU C, CHENG Q, et al., (2005) Experimental investigations on visualization of three-dimensional temperature distributions in a large-scale pulverized-coal-fired boiler furnace, Proc. Combust. Inst., 2005 30 p1699-1706; DOI: 10.1016/j.proci.2004.08.090.